PASJ: Publ. Astron. Soc. Japan **53**, 37–52, 2001 February 25

Exploring Galaxy Evolution from Infrared Number Counts and Cosmic Infrared Background

Tsutomu T. TAKEUCHI
Division of Particle and Astrophysical Sciences, Nagoya University, Chikusa-ku, Nagoya 464-8602
takeuchi@u.phys.nagoya-u.ac.jp
Takako T. ISHII
Kwasan and Hida observatories, Kyoto University, Yamashina-ku, Kyoto 607-8471
Hiroyuki HIRASHITA[1] and Kohji YOSHIKAWA[1]
Department of Astronomy, Kyoto University, Sakyo-ku, Kyoto 606-8502
Hideo MATSUHARA
The Institute of Space and Astronautical Sciences, Sagamihara, Kanagawa 229-8510
Kimiaki KAWARA
Institute of Astronomy, The University of Tokyo, Mitaka, Tokyo 181-0015
and
Haruyuki OKUDA
Gunma Astronomical Observatory, Nakayama, Takayama, Agatsuma, Gunma 377-0702

(Received 2000 June 6; accepted 2000 September 19)

Abstract

Recently reported infrared (IR) galaxy number counts and cosmic infrared background (CIRB) all suggest that galaxies have experienced strong evolution sometime in their lifetime. We statistically estimate the galaxy evolution history from these data. We find that an order-of-magnitude increase of the far-infrared (FIR) luminosity at redshift $z = 0.5$–1.0 is necessary to reproduce the very high CIRB intensity at 140 μm reported by Hauser et al. (1998, AAA 070.161.559) and decreases to, even at most, a factor of 10 toward $z \sim 5$, though many variants are allowed within these constraints. This evolution history also satisfies the constraints from the galaxy number counts obtained by IRAS, ISO and, roughly, SCUBA. The rapid evolution of the comoving IR luminosity density required from the CIRB well reproduces the very steep slope of galaxy number counts obtained by ISO. We also estimate the cosmic star formation history (SFH) from the obtained FIR luminosity density, considering the effect of the metal enrichment in galaxies. The derived SFH increases steeply with redshift in $0 < z < 0.75$, and becomes flat or even declines at $z > 0.75$. This is consistent with the SFH estimated from the reported ultraviolet luminosity density. In addition, we present the performance of the Japanese ASTRO-F FIR galaxy survey. We show the expected number counts in the survey. We also evaluate how large a sky area is necessary to derive secure information of galaxy evolution up to $z \sim 1$ from the survey, and find that at least 50–300 deg^2 is required.

Key words: galaxies: active — galaxies: evolution — galaxies: formation — galaxies: starburst — infrared: galaxies

1. Introduction

Galaxy evolution has long been a strong driving force of cosmological studies, and many problems still remain unsolved. Not only optical but also infrared (hereafter IR) and submillimeter (sub-mm) waveband observations of galaxies are of crucial importance for a full understanding of their evolutionary status.

Recent infrared and sub-mm surveys have revealed very steep slopes of galaxy number counts compared with that expected from the no-evolution model, and have provided a new impetus to related fields (e.g. Kawara et al. 1998; Puget et al. 1999; Dole et al. 2000; Oliver et al. 2000a; Kawara et al. 2000; Okuda 2000). The 170-μm slope proved to be $d \log N / d \log S \lesssim -2.5$ at $S \simeq 0.5$ Jy in these new deep surveys, while the slope would be ~ -1.5 in the no-evolution case. Such an excess of galaxy number count is generally understood to be a consequence of strong galaxy evolution, i.e. a rapid change in the star-formation rate in galaxies.

Another important related issue is the cosmic infrared background (CIRB), which is the integrated IR light from galaxies, especially from those that are too faint to be resolved. Therefore, the CIRB provides important information on the past star-formation history of galaxies including inaccessible sources. The CIRB has been detected by COBE (Puget et al. 1996; Fixsen et al. 1998; Hauser et al. 1998). The reported CIRB intensity is surprisingly high ($\nu I_\nu = 25 \pm 7\,\mathrm{nWm^{-2}sr^{-1}}$ at 140 μm and $\nu I_\nu = 14 \pm 3\,\mathrm{nWm^{-2}sr^{-1}}$ at 240 μm: Hauser et al. 1998), and has provided a profound problem awaiting to be solved.

Now, next-generation space infrared facilities (e.g. ASTRO-F, SIRTF, NGST, and FIRST) are scheduled, and we can expect a vast amount of novel observational knowledge with unprecedented precision. Among the above-

[1] Research Fellows of the Japan Society for the Promotion of Science.

mentioned facilities, ASTRO-F (Infrared Imaging Surveyor: IRIS) is a Japanese infrared satellite which will be launched in 2004.[2] In order to calculate the expected detection number in the survey planned for the ASTRO-F project, we have made a simple empirical model for the galaxy number count (Takeuchi et al. 1999; Hirashita et al. 1999). The applied model is based on the IRAS surveys. Therefore, though our previous model has successfully worked, it cannot reproduce the observed slopes of the novel ISO source counts, and the evolutionary effect is no longer satisfactorily estimated. We thus need an improved model to study the detailed observational plans and follow-up strategies at other wavelengths.

There have been a number of attempts to predict the IR–sub-mm source counts or the CIRB properties. Modeling methods of the source counts and the CIRB roughly fall into two categories. One is the backward approach, which is based on the local far-IR (FIR) luminosity function (LF) and the observed spectral energy distribution (SED) of galaxies in the FIR–sub-mm, with the assumptions of simple functional forms for the evolution (e.g. Beichman, Helou 1991; Pearson, Rowan-Robinson 1996; Malkan, Stecker 1998; Xu et al. 1998; Takeuchi et al. 1999). The other is the forward approach, which is based on models constructed by detailed processes related to the evolution of galaxies with a number of parameters (e.g. Franceschini et al. 1994; Guiderdoni et al. 1998). Tan, Silk, and Balland (1999) presented an interesting approach to combine the two methods. Because these two different approaches have their own merits and demerits, they must interplay with each other.

In this paper, we apply the backward empirical approach to derive the evolution of FIR properties of galaxies, but assume no specific functional form for the evolution history. Instead, we treat the galaxy evolution as a stepwise nonparametric form and search for the most plausible solutions, which well reproduce both the available IR galaxy number counts and the remarkable spectrum of the CIRB in a consistent manner.

The remainder of this paper is organized as follows. We give a model description and formulation in section 2. We illustrate the method of our analysis in section 3. In section 4 we show the most probable solutions to explain the observed IR number counts and CIRB. Some discussions are presented in section 5. Section 6 is devoted to our conclusions. We present the expected number counts of the ASTRO-F FIR all-sky survey in the appendix. Throughout this paper we use the following cosmological parameter set, unless otherwise stated: $H_0 = 75$ km s^{-1} Mpc^{-1}, $q_0 = 0.1$, and $\lambda_0 = 0$.

2. Model Description

The galaxy number count model is represented by SED, LF, cosmology, and galaxy evolution. We review the framework of the number count model and discuss these ingredients for our model in this section.

[2] Detailed information concerning the ASTRO-F mission is available at http://www.ir.astro.isas.ac.jp/ASTRO-F/index-e.html.

2.1. Spectral Energy Distribution

The infrared–radio galaxy SED is modeled by a superposition of the following components. For the infrared–sub-mm component, we consider PAH (polycyclic aromatic hydrocarbon), graphite, and silicate dust spectra (Dwek et al. 1997). In the case of the radio-quiet sources, the emission at the millimeter wavelength regime is dominated by the synchrotron radiation explained by supernova remnants (Condon 1992).

By considering the above, we start to construct the infrared model SEDs based on the IRAS color–luminosity relation (Smith et al. 1987; Soifer, Neugebauer 1991). Smith et al. (1987) and Soifer, Neugebauer (1991) found that the IRAS FIR colors and FIR luminosity are tightly correlated. The FIR color–60-μm luminosity relation derived by Smith et al. (1987) is

$$\log \frac{S_{60}}{S_{100}} = (0.10 \pm 0.02) \log L_{60} - (1.3 \pm 0.2)\,, \tag{1}$$

where S_λ is the detected flux density at wavelength λ [μm], and L_{60} [$L_\odot$] is the intrinsic luminosity evaluated at the 60-μm bandpass, $L_{60} \equiv \nu L_\nu$ at 60 μm. The relation reported by Soifer and Neugebauer (1991) is slightly nonlinear, but is also a monotonic function of L_{60}. We interpreted this relation to be the dust temperature $T_{\rm dust}$–L_{60} relation and calculated the modified blackbody continuum with the corresponding $T_{\rm dust}$. We adopted the dust emissivity $\varepsilon_\nu \propto \nu^\gamma$ with $\gamma = 1.0$, 1.5, and 2.0, and found that these three values yield only a small difference ($\lesssim 10\%$) in the $T_{\rm dust}$–L_{60} relation. We hereinafter use $\gamma = 1.5$.

We then utilized the data provided by Soifer and Neugebauer (1991) and derived the approximately linear relation between IRAS flux densities, S_{60} and S_{25}. The tight correlation between the FIR and mid-IR (MIR) flux is also found in the diffuse emission from the Galaxy by Infrared Telescope in Space (IRTS: Shibai et al. 2000). We thus added the mid-infrared spectra proposed by Dwek et al. (1997) to the FIR component so that the superposed spectra reproduce the correlation reported by Smith et al. (1987), such that $\log S_{25}/S_{60} \simeq -0.9$. The unidentified infrared bands (UIBs), which we assumed to be produced by PAHs, are also an important component of the IR SEDs of galaxies. We set the continuum-to-band intensity ratio as reported by Dwek et al. (1997). Detailed properties of PAHs are taken from Allamandola et al. (1989), e.g. we set the PAH features at 3.3 μm, 6.2 μm, and 7.7 μm with a broader component at 5.5–9.5 μm and 11.3 μm.

A remarkably tight and ubiquitous correlation is well-known between the FIR continuum flux and the radio continuum flux (e.g. Helou et al. 1985; Bregman et al. 1992; Condon 1992). For the longer wavelength regime, a power-law continuum produced by synchrotron radiation ($\propto \nu^{-\alpha}$) dominates the observed emission. We set $\alpha = 0.7$ according to Condon (1992), and added the FIR composite spectra, using the relation

$$q \equiv \log\left(\frac{\rm FIR}{3.75 \times 10^{12}\ {\rm W m^{-2}}}\right) - \log\left(\frac{S_{1.4\,{\rm GHz}}}{\rm W m^{-2} Hz^{-1}}\right) = 2.3, \tag{2}$$

where

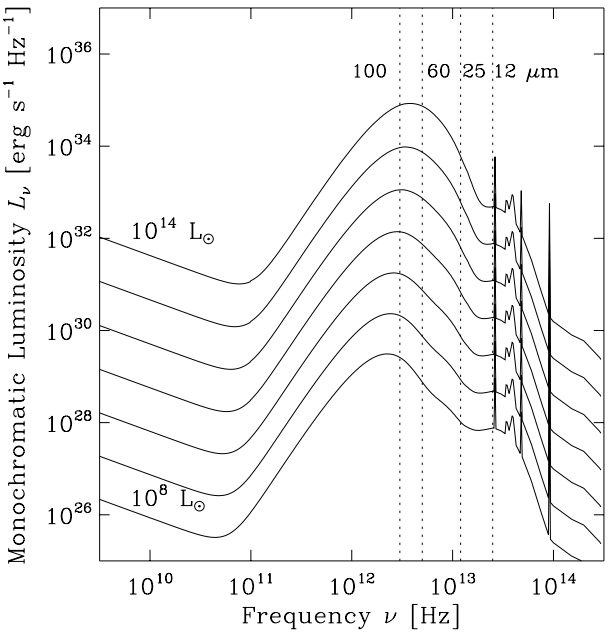

Fig. 1. Assumed galaxy spectral energy distribution in the near infrared to radio wavelengths, constructed from the color–luminosity evolution in IRAS galaxies and the tight correlation of the far-infrared (FIR) and radio fluxes. The prominent emission bands are PAH features. The vertical dotted lines represent the wavelengths of IRAS four bandpasses. The SEDs with the FIR luminosity of 10^8, 10^9, 10^{10}, 10^{11}, 10^{12}, 10^{13}, and 10^{14} $L_\odot$ are shown from the bottom in this order.

$$\mathrm{FIR}\,[\mathrm{Wm}^{-2}] \equiv 1.26\times10^{-14}\,(2.58\,S_{60}\,[\mathrm{Jy}] + S_{100}\,[\mathrm{Jy}])$$

(Condon 1992). Equation (2) is adopted in Helou et al. (1988) and will be applied again in section 5. This is the final SED we use in our number count and CIRB models (see figure 1).

2.2. *Local Luminosity Function and Evolutionary Effect*

We adopted the 60-μm LF based on the IRAS by Soifer et al. (1987) as the local IR LF of galaxies:

$$\log\phi_0(L_{60}\,[L_\odot]) = \begin{cases} 4.87 - 0.73\log L_{60}\,[L_\odot] & \text{for } 10^8 < L_{60} < 10^{9.927}, \\ 18.5 - 2.1\log L_{60}\,[L_\odot] & \text{for } 10^{9.927} < L_{60} < 10^{13}, \\ \text{no galaxies} & \text{otherwise}, \end{cases} \quad (3)$$

where ϕ_0 is the number density of galaxies in $\mathrm{Mpc}^{-3}\,\mathrm{dex}^{-1}$. We show the LF in the upper panel of figure 2. We applied the double power-law form for the local LF. The lower cut-off luminosity do not seriously affect the result, as stated in Takeuchi et al. (1999). The effect of the faint-end slope of the LF on the number-count estimation is briefly summarized in Takeuchi, Shibai, and Ishii (2000a).

We assumed a pure luminosity evolution in this study. In this case, the 60-μm luminosity of a certain galaxy at redshift z is described as

$$L_{60}(z) = L_{60}(0)\,f(z)\,. \quad (4)$$

We also assumed that the luminosity evolution is 'universal', i.e. independent of galaxy luminosity. This is depicted in the lower panel of figure 2. In the previous backward approach, a certain functional form of $f(z)$ was often assumed for the

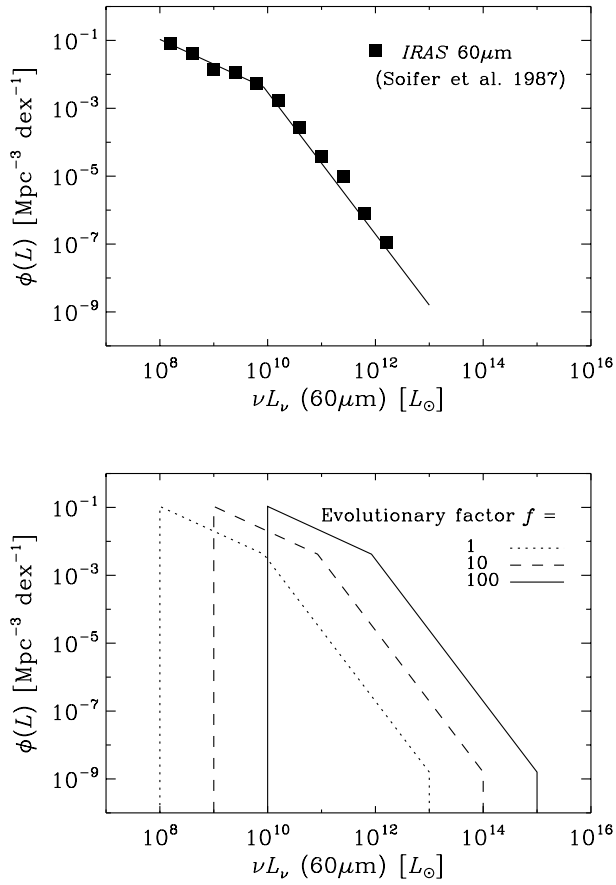

Fig. 2. Upper panel: the applied 60-μm luminosity function (LF) in this paper. This LF is derived by Soifer et al. (1987). Lower panel: a schematic representation of its evolution as a function of redshift.

evolution of galaxies, and model counts were calculated and compared with observations. We, on the contrary, treat the evolution of galaxy luminosities as a stepwise nonparametric form which is to be statistically estimated, in order to explore the most suitable evolutionary history which reproduces the present observational results. Mathematically, we regard the evolution estimation from the number count as an inverse problem, and apply the universal LF evolution in order to obtain a statistically stable solution. The constraints of $f(z)$ from the observed CIRB spectrum are given in subsection 4.1. Another approach mainly based on density evolution is discussed in Pearson et al. (2000). We note that the present quality of the IR number count data is not sufficient to estimate the evolution of the shape of the LF, and fine tuning of the LF shape is less meaningful. Such work remains to be solved after a forthcoming release of huge databases.

2.3. *Formulation of the Galaxy Number Count*

Using the above formulae, now we calculate the flux–number ($\log N$–$\log S$) relation, or the so-called galaxy number count. We assume that galaxies can be regarded as point sources (i.e. the cosmological dimming of the galaxy surface brightness is not taken into account). Then, the relation between the observed flux $S(\nu)$ and the emitted monochromatic luminosity $L(\nu_{\mathrm{em}}) = L[(1+z)\nu]$ is given by

$$S(\nu) = \frac{(1+z)L\left[(1+z)\nu\right]}{4\pi d_{\rm L}^2}, \quad (5)$$

where $d_{\rm L}$ is the luminosity distance. When we fix a certain $S(\nu)$, we obtain $L[(1+z)\nu]$ by using equation (5). Then, the corresponding $L_{60}[S(\nu), z]$ at a redshift of z is uniquely determined. We define $N[> S(\nu)]$ as the number of galaxies with a detected flux density larger than $S(\nu)$ in a survey solid angle Ω; it is then formulated as

$$N[> S(\nu)] = \int_\Omega d\Omega \int_0^{z_{\rm max}} dz \frac{d^2V}{dz\, d\Omega} \times \int_{L_{60}[S(\nu),z]}^{\infty} \phi(z,\, L'_{60})\, dL'_{60}\,, \quad (6)$$

where $d^2V/dzd\Omega$ is the comoving volume element per sr, and $z_{\rm max}$ is the maximum redshift which we consider in this study. As shown later, we set $z_{\rm max} = 5$.

We then formulate the number count with the evolution. If pure luminosity evolution takes place, by using equation (4), the evolution of the luminosity function with redshift is expressed as

$$\phi(z, L_{60})\, dL_{60} = \phi_0 \left[\frac{L_{60}}{f(z)}\right] d\left[\frac{L_{60}}{f(z)}\right], \quad (7)$$

where $\phi_0(L_{60})$ is the IR LF in the local Universe. The expected number count is expressed as

$$\begin{aligned} N[> S(\nu)] &= \int_\Omega d\Omega \int_0^{z_{\rm max}} dz \frac{d^2V}{dz\, d\Omega} \times \int_{L_{60}[S(\nu),z]}^{\infty} \phi_0 \left[\frac{L_{60}{}'}{f(z)}\right] d\left[\frac{L_{60}{}'}{f(z)}\right] \\ &= \int_\Omega d\Omega \int_0^{z_{\rm max}} dz \frac{d^2V}{dz\, d\Omega} \times \int_{L_{60}[S(\nu),z]/f(z)}^{\infty} \phi_0(\tilde{L}'_{60})\, d\tilde{L}'_{60}\,, \end{aligned} \quad (8)$$

where $\tilde{L}_{60} = L_{60}/f(z)$. The full formulation of the galaxy number count, including a density evolution, is given in e.g. Gardner (1998) or Takeuchi et al. (1999). In this paper we call $f(z)$ 'the evolutionary factor'.

2.4. *Formulation of the Cosmic Infrared Background*

The CIRB is generated from the integrated light of galaxies. Therefore, combining the SEDs of galaxies and the number count predictions, we obtain the CIRB spectrum. The observed flux density of a galaxy whose IR luminosity is L_{60}, and $S(\nu, L_{60})$ is given by equation (5) as follows:

$$S(\nu\,, L_{60}) = \frac{(1+z)L\left[\nu(1+z)\,, L_{60}\right]}{4\pi d_{\rm L}^2}, \quad (9)$$

where $L(\nu, L_{60})$ is the monochromatic luminosity of a galaxy with L_{60}. Then, the CIRB spectrum $I(\nu)$, i.e., the background flux density from a unit solid angle, is expressed as

$$I(\nu) = \int_0^{z_{\rm max}} dz \frac{d^2V}{dz\, d\Omega} \int_0^{\infty} \phi(z,\, L'_{60}) S(\nu\,,\, L'_{60})\, dL'_{60}\,. \quad (10)$$

We can deal with the evolutionary effect on $I(\nu)$ through $\phi(z, L_{60})$, just the same as in the case of the number-count calculation.

3. Analysis

In principle, the galaxy number count and the spectral shape of the CIRB are integrated values along with the redshift. Therefore, the information of galaxy evolution with the redshift is degenerate if we analyze a dataset obtained from a single wavelength. But the redshift degeneracy can be solved by treating the multiband observational results at the same time as suggested by Takeuchi et al. (2000b), who studied the changes in the IR number counts against some extreme galaxy-evolution histories.

Here, we thoroughly survey the response of the multiband number counts and the CIRB to the change of the evolutionary factor at various redshifts. We first divide the redshift into the following eight intervals: [0–0.25], [0.25–0.5], [0.5–0.75], [0.75–1.0], [1.0–1.5], [1.5–2.0], [2.0–3.0], and [3.0–5.0]. If we set the evolutionary factor $f(z) = 10$ at each interval, the number counts and the CIRB will deviate from the no-evolution prediction differently, corresponding to each interval. This different response of the predictions provides useful information of the evolution with a redshift. For example, consider a certain deviation in the number count at one waveband. Without any other information, we cannot distinguish a certain evolution history from all other possibilities. But, when we use the deviations at other wavelengths and in the CIRB, we can check the validity of the evolution by the goodness-of-fit to the data at other wavelengths, and may infer a much more constrained parameter range.

We show the deviations of the CIRB spectrum and the galaxy number counts with an order-of-magnitude evolution at each redshift interval in figures 3 and 4. The left-hand panel of figure 3 depicts the response of the CIRB spectrum for a hypothetical order-of-magnitude evolution at the above-mentioned redshift interval at $z < 1$. The no-evolution prediction of the CIRB is presented by the thick solid curve. The dotted line represents the CIRB when $f(z) = 10$ at $0 < z < 0.25$, the dashed line at $0.25 < z < 0.5$, the dot-dashed line at $0.5 < z < 0.75$, and the dot-dot-dot-dashed line at $0.75 < z < 1.0$, respectively, in figure 3. The peak of each CIRB model prediction shifts toward longer wavelengths, with the increasing redshift of the input test evolution, while the intensity of the CIRB at the sub-mm regime is insensitive to the evolution at $z < 1$. On the other hand, the right-hand panel of figure 3 illustrates the response of the CIRB caused by each test evolution at $z > 1$. This time the dotted line represents the CIRB when $f(z) = 10$ at $1.0 < z < 1.5$, the dashed line at $1.5 < z < 2.0$, the dot-dashed line at $2.0 < z < 3.0$, and the dot-dot-dot-dashed line at $3.0 < z < 5.0$, respectively. Again, the thick solid line is the no-evolution prediction. At $z > 1$, the evolution mainly affects the intensity of the sub-mm CIRB spectrum.

How about the number count? We show the effect of the test evolution on the multiband number counts in figure 4. The response galaxy number counts at 15 μm, 60 μm, and 90 μm are displayed in figure 4a, while those at 170 μm, 450 μm, and 850 μm are in figure 4b. The same as in figure 3, the response of the number counts for the input test evolution at $z < 1$ are indicated in the left-hand panels, and that for the input evolutions at $z > 1$ in the right-hand panels, in figures 4a and b.

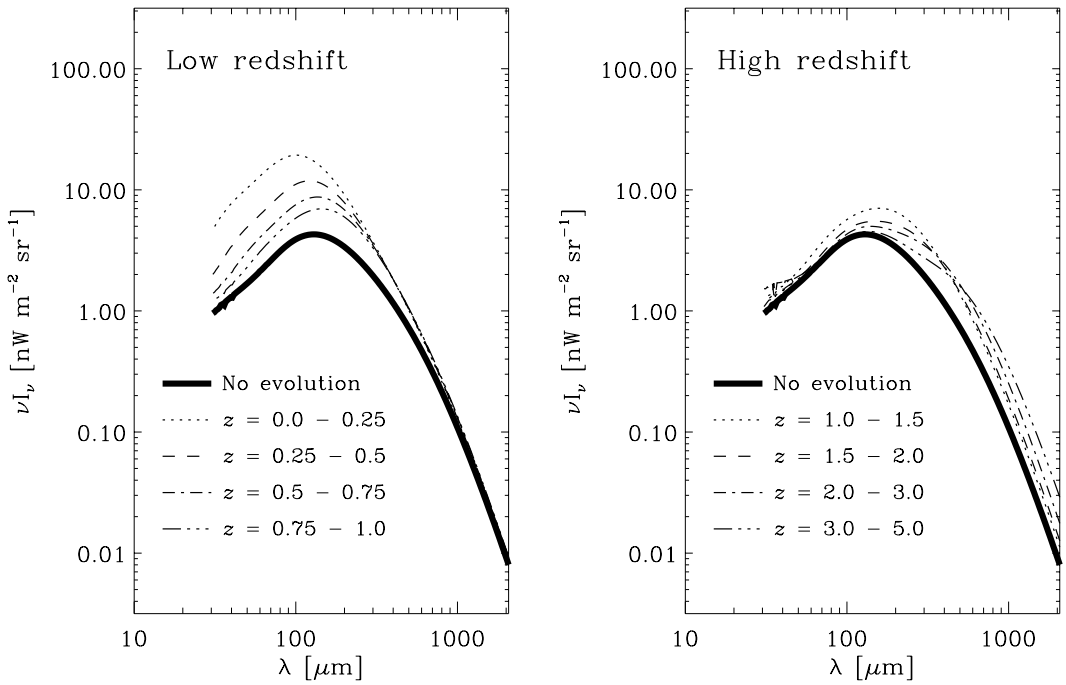

Fig. 3. Deviations of the CIRB spectrum and the galaxy number counts with an order-of-magnitude evolution at the following eight intervals: [0–0.25], [0.25–0.5], [0.5–0.75], [0.75–1.0], [1.0–1.5], [1.5–2.0], [2.0–3.0], and [3.0–5.0]. The left panel depicts the response of the CIRB spectrum for hypothetical, an order-of-magnitude evolution at the above redshift interval at $z < 1$. The no-evolution prediction of the CIRB is presented by the thick solid curve. The right panel illustrates the response caused by each test evolution at $z > 1$.

We can clearly see that the MIR 15-μm count is almost independent of the status of galaxies at $z \gtrsim 0.75$, and it is quite sensitive to the evolution at $0.25 < z < 0.5$. Thus, the 15-μm galaxy number count is a useful and unique indicator of the evolution at such low redshifts. The 60-μm count still depends strongly on the evolution at $0.25 < z < 0.5$, and is more sensitive to the evolutionary status at $0.5 < z < 0.75$. On the contrary, it is insensitive to that at $z \gtrsim 1$. This trend of the redshift dependence becomes more prominent at FIR 90- and 170-μm number counts. The effect of the evolution at $1.0 < z < 1.5$ begins to appear in the faintest slope of the number counts at these wavelengths. The sub-mm 450- and 850-μm counts show, in contrast, a weaker dependence on the low-z ($z < 1$) galaxy evolution. They are very strongly dependent on the evolutionary factor at $z \gtrsim 1$. Here, notice that the effect of the test evolution at $z > 1$ is almost constant at 850 μm. This is caused by the counter-intuitive, negative K-correction.

In summary, we are able to resolve the degeneracy of the galaxy evolution history by treating the multiband datasets and the CIRB at the same time. Since the amplitude of the evolutionary factor at various redshift intervals correlates with each other, this statistical inference problem is still more difficult than a mere fitting problem. But we can obtain a set of permitted ranges of the evolutionary factors as a function of the redshift by this method.

4. Results

In figure 5, we summarize the observational constraints of the evolutionary factor estimated from the IR galaxy number counts and the CIRB. The thick dashed horizontal lines depict the bounds mainly based on the IR galaxy number counts. The thick solid lines are the constraints based on both CIRB and IR number counts. The thick dot-dashed line is determined by the severe constraints from the CIRB spectrum at sub-mm wavelengths. We set that there are no galaxies at $z > 5$. Although this is not a strict observational constraint, the observed CIRB suggests that there are few luminous IR galaxies at such a high redshift. We explain and discuss the details of these constraints in the following.

4.1. Constraint from Cosmic Infrared Background

Today, we have considerable information on the spectrum of the CIRB. As we mentioned in section 1, the CIRB has been revealed to have a surprisingly high intensity at the FIR wavelength regime ($\nu L_\nu = 25 \pm 7\,\mathrm{nWm^{-2}sr^{-1}}$ at 140 μm and $\nu L_\nu = 14 \pm 3\,\mathrm{nWm^{-2}sr^{-1}}$ at 240 μm: Hauser et al. 1998). Thus, the spectral shape of the CIRB can be used to constrain the evolutionary history of the cosmic IR luminosity density, which is closely related to the cosmic history of star formation and metal production.

We summarize the reported intensity of the CIRB in figure 6. The open squares with downward arrows represent the "dark sky" upper limit to the CIRB measured by COBE Diffuse Infrared Background Experiment (DIRBE). The DIRBE sky brightness varies roughly sinusoidally over a year, due to the complex features of the interplanetary dust cloud. The "dark sky" brightness is that of the darkest area on the sky at each wavelength. The open squares with upward arrows represent the residual signal of DIRBE after removing the contri-

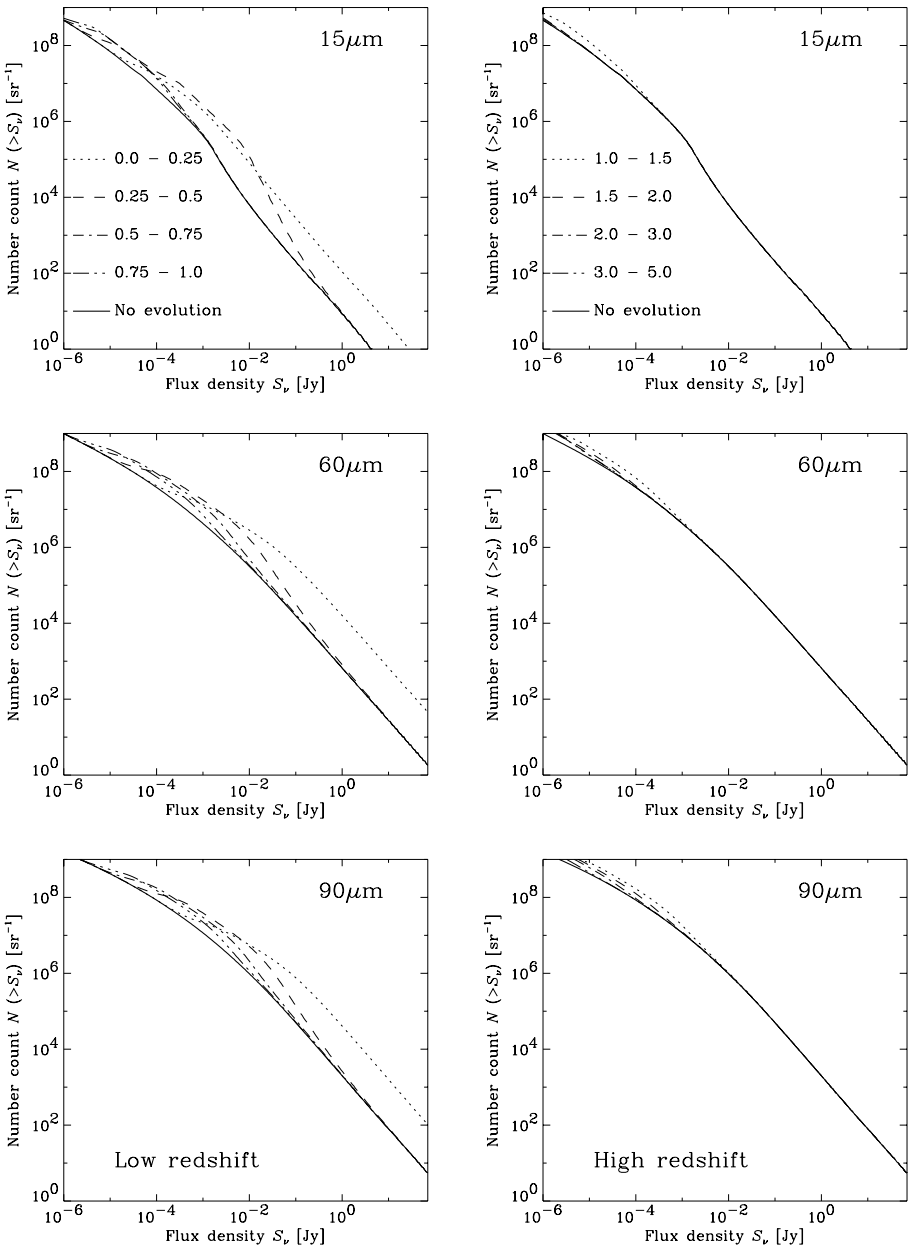

Fig. 4a. Effect of the test evolution to the multiband number counts. The response galaxy number counts at 15 μm, 60 μm, and 90 μm are displayed. The same as in figure 3, the response of the number counts for the input test evolution at $z < 1$ are indicated in the left panels, and that for the input evolutions at $z > 1$ in the right panels.

butions from the model foreground sources, such as galactic diffuse emission, and interplanetary dust emission. The filled squares with error bars are the DIRBE detections at 140 μm and 240 μm by Hauser et al. (1998). The hatched region is the permissible range derived from the COBE Far Infrared Absolute Spectrophotometer (FIRAS) high-frequency data, after removing the cosmic microwave background (CMB) signal (Fixsen et al. 1998). At wavelengths shorter than 140 μm, the strong emission from the interplanetary dust prevents us from estimating a reliable value of the extragalactic component; therefore, in this study we do not use the intensity at this wavelength range recently reported by some authors. The detector noise level of DIRBE becomes worse at wavelengths longer than 240 μm. On the other hand, the CIRB spectrum at the sub-mm regime detected by FIRAS is considered to be highly robust, because in this wavelength regime, what to be subtracted is only the blackbody spectrum of the CMB, which has no model ambiguity.

Lagache et al. (1999) claim that, from their observation of the sky in and around the Lockman Hole, there exists a significant contribution from the galactic warm interstellar medium (WIM) to the IR background intensity. Thus, if we adopt their interpretation, the CIRB intensities become $15.3 \pm 6.4\,\mathrm{nW^{-2}sr^{-1}}$ (140 μm) and $11.4 \pm 1.9\,\mathrm{nW^{-2}sr^{-1}}$ (240 μm). The contribution of the WIM at sub-mm wavelength is small, and the intensity of the CIRB at 200–2000 μm is almost

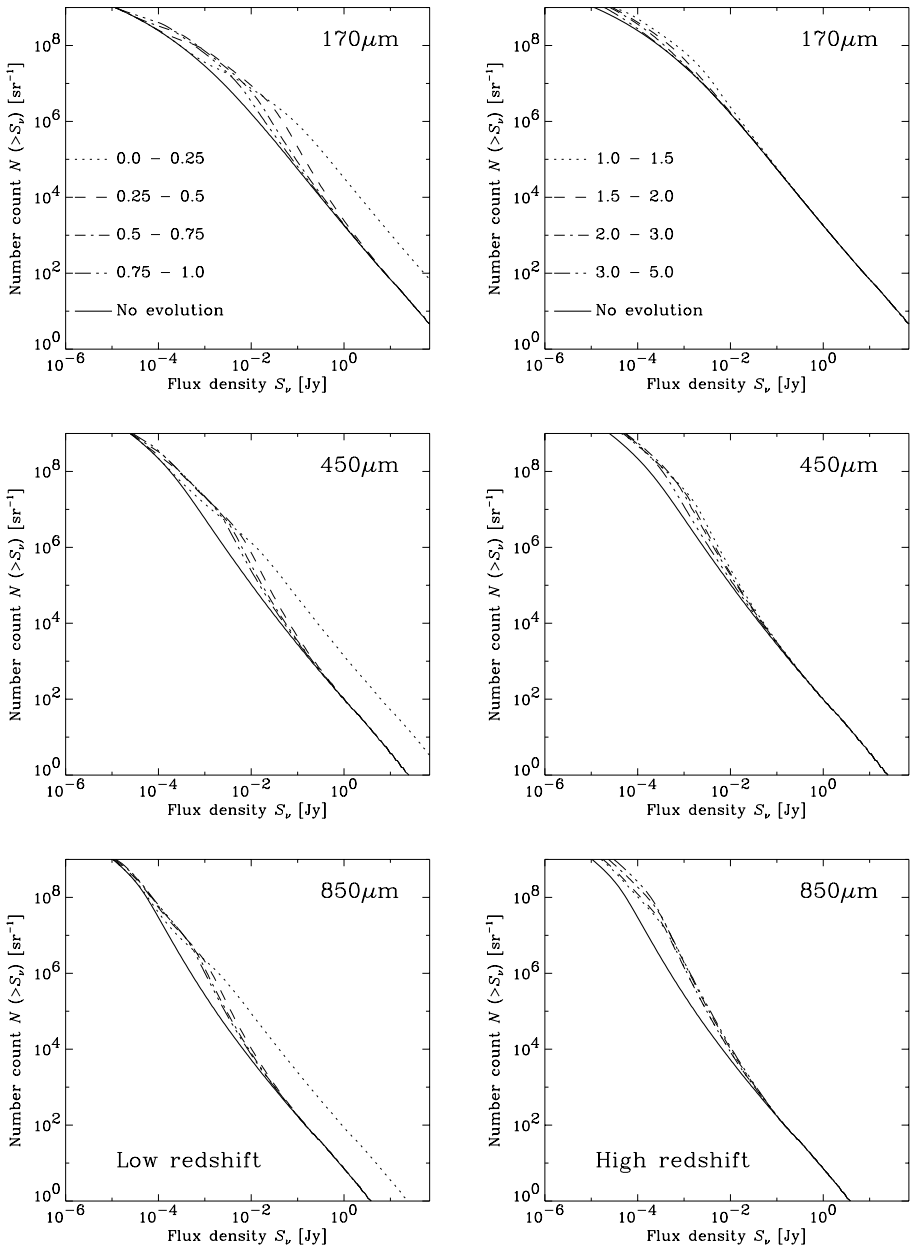

Fig. 4b. Same as figure 4a, except that these counts are at 170 μm, 450 μm, and 850 μm.

unchanged from Fixsen et al.'s value. However, in other regions, Lagache et al. (2000) reported similar results to Hauser et al. (1998), even though they again consider the contributions of the WIM, and the existence of the WIM still seems to be a matter of debate. We present the claimed value of Lagache et al. (1999) by filled triangles with errors in figure 6.

Upon glancing at figure 6, it is obvious that no evolution prediction is strongly ruled out. The CIRB intensity at 140 μm suggests an order-of-magnitude evolution of IR galaxies. It is important that such a short wavelength of the CIRB peak can only be reproduced by a rapid evolution of galaxies at low redshift ($z < 1$). Even if we use the slightly lower value of Lagache et al. (1999), this conclusion is not affected. If we try to explain the peak intensity by high-redshift IR galaxies, vast numbers of galaxies are required. Furthermore, if in case, the CIRB intensities at longer wavelengths are overpredicted, the observed spectrum would be seriously violated. As we noted, because the FIRAS spectrum at sub-mm wavelength is highly reliable, all of the model must reproduce it exactly. At least, models which overestimate the FIRAS spectrum should be dismissed. The sub-mm slope of the CIRB is shallower compared with a single galaxy SED, which should be interpreted as an integrated SED of a significant number of galaxies at high redshift ($z > 2$–3) (see figure 3). Thus, though the constraint is strong, it is not inconsistent with the actual existence of obscured high-z starbursts (e.g. Hughes 2000; Ishii et al. 2000). What we should stress is that there is an observational upper bound of the evolution of IR galaxies. In figure 5, the con-

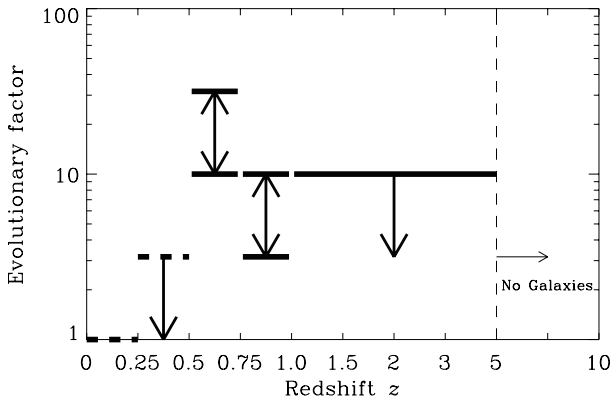

Fig. 5. Summary of the constraints of the galaxy luminosity evolution inferred from the infrared galaxy number counts and the cosmic infrared background radiation spectrum.

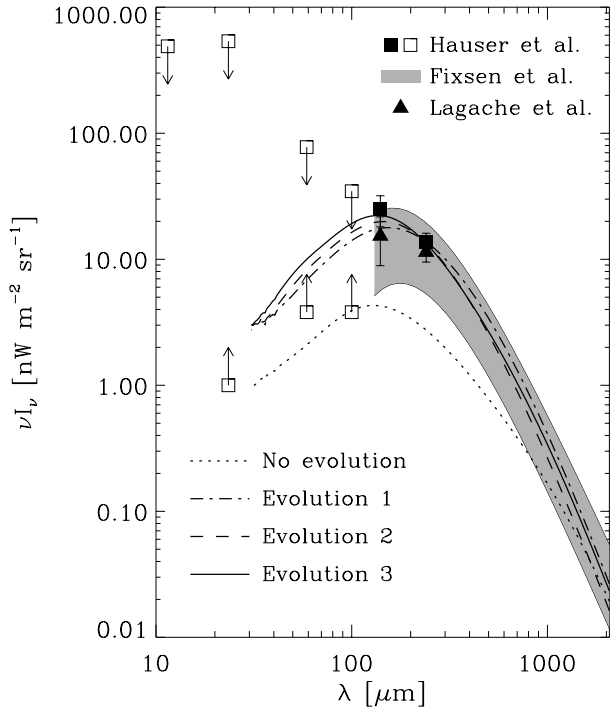

Fig. 6. Cosmic infrared background observations and our model predictions. The dotted line describes the no-evolution prediction. The dot-dashed line shows the model CIRB with Evolution 1, the dashed line represents the CIRB with Evolution 2, and the solid line with Evolution 3, respectively.

straints from the CIRB peak intensity is presented as an enhancement of the evolutionary factor at $0.5 < z < 0.75$, and the constraints from FIRAS observation are shown by the upper bound at $1 < z < 5$.

Hereafter, within the permitted range derived from the CIRB, we focus on the three representative evolutionary histories. We show these evolutions in figure 7. Evolution 1 has a steep rise at $0 < z < 0.5$, reaches the summit at which the evolutionary factor $f(z)$ is 10, and has a plateau at $0.5 < z < 2$. Then, at $2 < z$, the evolutionary factor slowly decreases, but is still higher than the local value. This rather moderate evo-

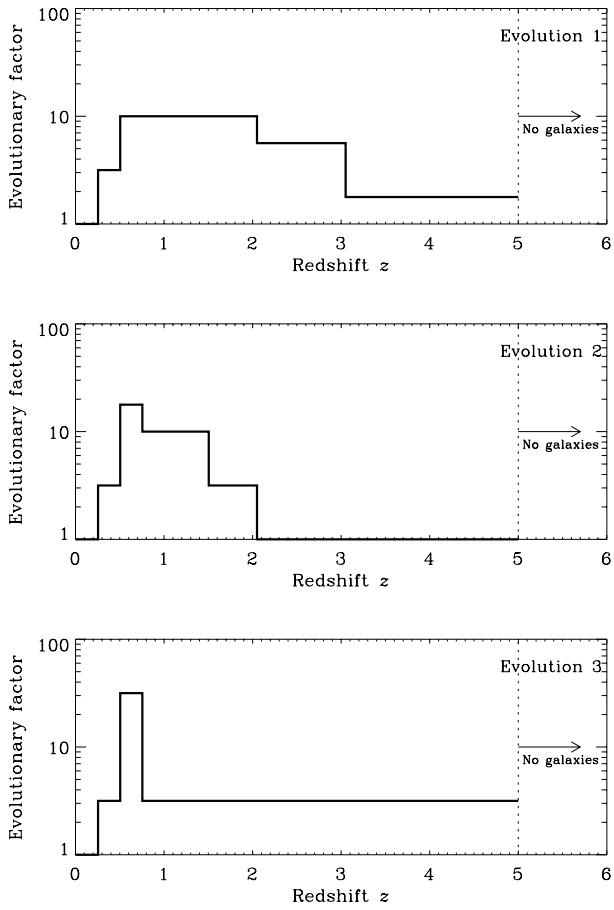

Fig. 7. Three representative galaxy evolutionary histories permitted by the observational constraints presented in figure 5.

lution is consistent with the CIRB 140-μm intensity when we consider the WIM contribution, and slightly overestimates the FIRAS sub-mm spectrum. These features are also described in figure 6 as the dot-dashed line.

Evolution 2 has a stronger rise of the evolutionary factor than Evolution 1 at $0 < z < 0.5$. Beyond the peak at $0.5 < z < 0.75$, the evolutionary factor decreases rapidly to the local value at $z < 2$, and at $2 < z < 5$ the IR LF is the same as the local one. This evolution mitigates the overestimation of the sub-mm CIRB, and the 140-μm peak intensity has an intermediate value between Hauser et al. (1998) and Lagache et al. (1999).

Finally, Evolution 3 has the strongest rise at $0 < z < 0.5$. This evolution model has a prominent peak at $0.5 < z < 0.75$, which well reproduces the 140-μm peak of the CIRB by Hauser et al. (1998). This evolution also has a long plateau at $0.75 < z < 5$. The predicted CIRB by this model is quite consistent with the FIRAS spectrum. Since we present the evolutionary history as a function of the redshift, we would have an impression that the rise of the evolutionary factor at $0.5 < z < 0.75$ is unnaturally steep, but the peak height is 30 and the duration is ~ 2 Gyr, both of which are within the bounds of possibility and worth being considered.

These CIRB model behaviors are also shown in figure 6. No-evolution prediction is represented by the dotted line in figure 6. The dot-dashed line is the model CIRB produced by

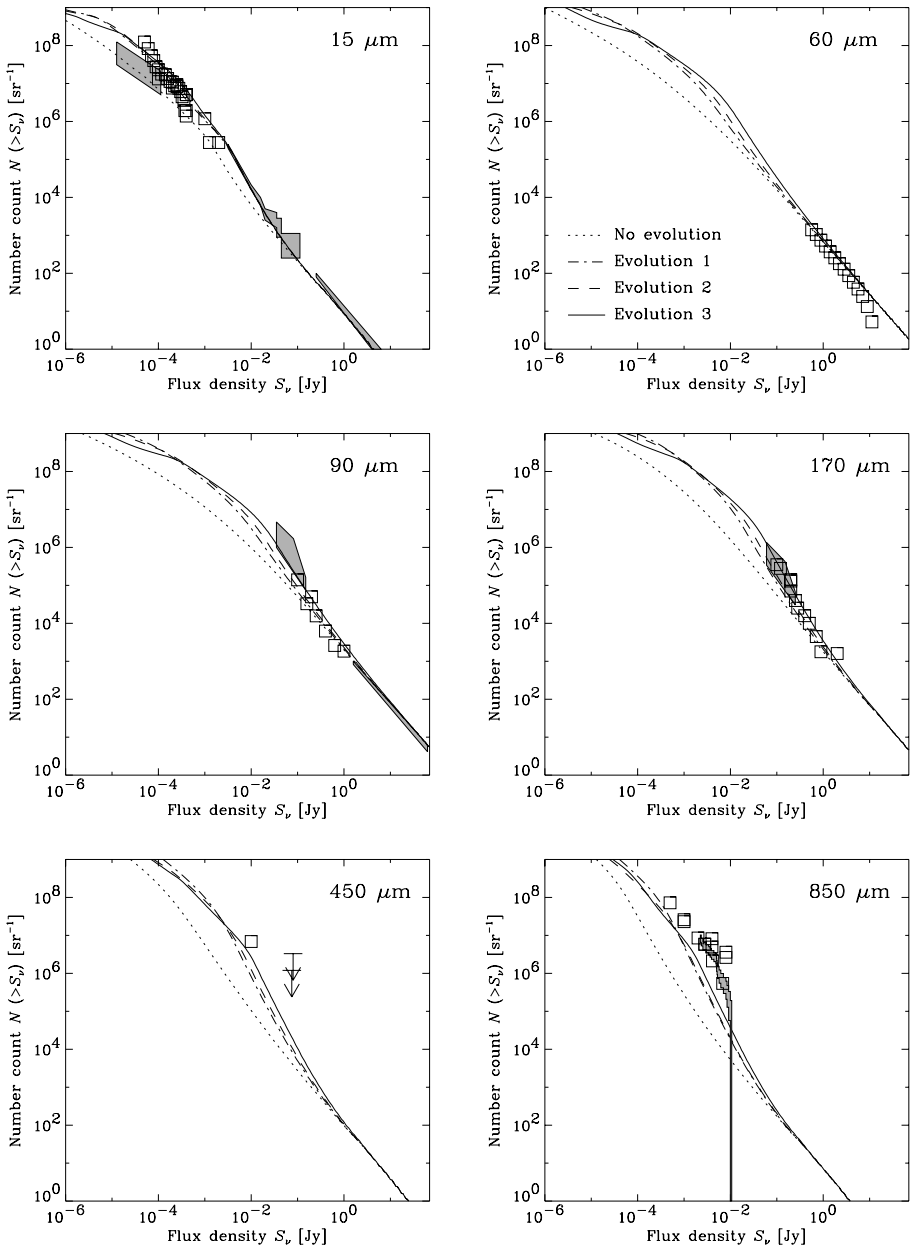

Fig. 8. Multiband galaxy number count at infrared–sub-mm wavelengths. Same as in figure 6, the dotted lines represent the no-evolution prediction. The dot-dashed lines are the counts with Evolution 1, the dashed lines are those with Evolution 2, and the solid lines with Evolution 3, respectively.

Evolution 1, the dashed line is that produced by Evolution 2, and the solid line is that Evolution 3.

4.2. Constraint from IR Galaxy Number Counts

We examine whether the three evolution models are consistent with observed galaxy number counts. Recently, new observational results of the galaxy number counts have become available at MIR, FIR, and sub-mm, mainly by the success of ISO (Infrared Space Observatory) and SCUBA (Submillimeter Common-User Bolometer Array for the James Clerk Maxwell Telescope). We are able to compile these data as well as previously obtained IRAS databases.

We present the galaxy number counts at 15–850 μm in figure 8. Again, the no-evolution predictions are represented by the dotted lines. The dot-dashed lines are the model number counts produced by Evolution 1, the dashed lines are produced by Evolution 2, and the solid line by Evolution 3, respectively. Here, we go into the details of the galaxy count at each wavelength in IR–sub-mm.

4.2.1. 15-μm galaxy number counts

The top-left panel of figure 8 shows the 15-μm galaxy counts predicted by our model with Evolutions 1, 2, and 3. We also show the available observed 15-μm ISOCAM galaxy counts (Flores et al. 1999a, b; Clements et al. 1999; Aussel et al. 1999; Altieri et al. 1999; Elbaz et al. 1999; Oliver et al. 2000a) and the constraint from fluctuation analysis [$P(D)$ analysis] of the Hubble Deep Field (HDF) (Oliver et al. 1997), together with

IRAS galaxy count (Rush et al. 1993). The observed counts are well reproduced by any of our three evolutionary histories, and clearly different from the no-evolution prediction. The slope and normalization of the IRAS count must be reproduced by a model *without any corrections*. The ELAIS (European Large-Area ISO Survey: Oliver et al. 2000a; for the present status, see http://athena.ph.ic.ac.uk) counts severely constrain the range of the evolutionary factor (Serjeant et al. 2000), and this shows that the rapid rise at $z < 0.75$ is necessary to explain the MIR galaxy number counts. Of course, too large an evolutionary factor is also forbidden by this data. The permitted range of the evolutionary factor is $f(z = 0.5\text{–}0.75) = 30 \pm 3$ if we take both the Poisson fluctuation and the cosmic variance into account (see appendix).

4.2.2. Far-infrared galaxy number counts

We next examine the galaxy counts at FIR wavelengths. The top-right panel of figure 8 is the IRAS 60-μm galaxy number count (Rowan-Robinson et al. 1991). Our model calculations are based on the statistical studies on the local IRAS galaxies and the IRAS 60-μm LF, the 60-μm count is automatically reproduced at the brightest end. On the other hand, the count at the faint flux limit restricts the evolution at lowest redshifts ($z \sim 0.1\text{–}0.3$). Some previous authors claimed having evidence of FIR galaxy evolution at the flux limit of IRAS (e.g. Saunders et al. 1990; Ashby et al. 1996; Bertin et al. 1997; Springel, White 1998), but the reported strengths of the evolution were not consistent with each other. We found that the evolutionary factor can be at most $f(z) < 3$ in the redshift range $0.25 < z < 0.5$; otherwise, the model number count could violate the 1-σ variance range of the observed IRAS count.

At 90 and 170 μm, deep galaxy counts are obtained by ISOPHOT. The photometric calibration of the ISO is still a matter of debate, and we should carefully consider the interpretation of the counts at these wavelengths. The middle-left panel presents our model 90-μm galaxy counts with observed FIRBACK source counts (Dole et al. 2000) and ISOPHOT CIRB project (Juvela et al. 2000), and the constraint from the fluctuation analysis of the ISO Lockman Hole data (Matsuhara et al. 2000). We also show the IRAS 100 μm galaxy counts by a hatched thin area at brightest flux. Again, our model shows excellent agreement with the IRAS count. The middle-right panel is the 170-μm galaxy counts. The observed counts are taken from Stickel et al. (1998), Kawara et al. (1998), Puget et al. (1999)(FIRBACK), Oliver et al. (2000b) (ELAIS), Juvela et al. (2000) and results of the fluctuation analysis of the Lockman Hole (Matsuhara et al. 2000). Most of these data suggest that the slope of the number counts is very steep, i.e. $d \log N / d \log S \lesssim -2.5$. This steep slope index strongly supports rapid evolution toward $z \sim 0.75$. This suggested evolution is quite consistent with the requirements of the CIRB spectrum.

We note that Evolutions 1, 2, and 3 show significant differences at 0.1–0.01 Jy in the FIR wavelength. Especially, only Evolution 3 can reproduce the constraint of Matsuhara et al. (2000). Thus, a huge database, such as the data of ASTRO-F all-sky survey, can discriminate this difference and fix the evolutionary history at this redshift regime ($0 \lesssim z \lesssim 0.75$).

4.2.3. Submillimeter galaxy number counts

The bottom-left and bottom-right panels of figure 8 show the 450- and 850-μm model number counts and observed counts obtained by SCUBA. It is now well accepted that the sub-mm source counts are suitable for examine the status of the high-redshift ($z > 1\text{–}2$) galaxies. The observed 450 μm counts were recently obtained by Blain et al. (2000), and two upper limits are based on Smail et al. (1997) and Barger, Cowie, and Sanders (1999). The symbols represent the observed 850 μm counts taken from Smail, Ivison, and Blain (1997), Hughes et al. (1998), Blain et al. (1999), Eales et al. (1999), and Holland et al. (1999), and the hatched region, Barger et al. (1998, 1999).

The 450-μm counts of Blain et al. (2000) can be reproduced by Evolution 3, because this evolutionary history has a long plateau toward $z = 5$. On the other hand, the 850-μm counts are somewhat problematic. If we attach importance to the FIRAS CIRB spectrum, our model slightly but significantly underestimates the source counts at 850 μm. We should consider the discrepancy found in our model predictions and detected sub-mm source counts because, in contrast our model successfully reproduced the FIRAS CIRB sub-mm spectrum. Since, in our estimate, IR galaxies are fewer at high redshift compared with sub-mm-weighted model (e.g. Tan et al. 1999), this result seems qualitatively natural.

Here, we consider the difficulty in measuring a source flux from noisy data. Hogg and Turner (1998) clearly summarize and discuss the upward bias of the flux estimation in the study of source number counts. Very recently Hogg (2000) extensively examined the confusion effect on the astrometric and photometric measurements. Hogg showed an important result that, if the observed number counts has a steep slope like IR and sub-mm source counts, a flux estimation must suffer from serious confusion noise and most of the faintest sources can be spurious. According to Hogg's discussion, the sampling strategies adopted in the field of sub-mm survey are often insufficient. Thus, we do not make any attempt to search for a solution which satisfies the present sub-mm source counts in this study. In order to settle this problem, a much better rule-of-thumb for the same flux limit level for the confusion is required. Eales et al. (2000) also performed a Monte Carlo simulation of the source extraction from the sub-mm images, and clearly showed that the estimated source fluxes are significantly boosted upwards, due to the heavy confusion.

We discuss another possible source of the sub-mm discrepancy. The hot gas in X-ray cluster of galaxies produces a spectral distortion of the CMB: the Sunyaev–Zel'dovich (SZ) effect (Sunyaev, Zel'dovich 1972). At wavelengths shorter than 1.38 mm, the SZ effect appears to be a positive source in the CMB and has a maximum intensity at 850 μm. The number count and redshift distribution of clusters are being actively studied by many authors (e.g. Barbosa et al. 1996; Kitayama et al. 1998). Kitayama et al. (1998) prediced sub-mm cluster number counts based on the Press–Schechter formalism (Press, Schechter 1974). The contribution of SZ clusters to the sub-mm numbers count is not negligible compared with the sub-mm galaxy counts, while their contribution to the CIRB is small (Kitayama et al. 1998). In addition, the SZ cluster is a diffuse source, and thus they might affect the flux estimation of sub-mm point sources in the cluster regions. Hughes and

Gatztañaga (2000) has already included the effect of the SZ clusters in their sub-mm sky image simulations.

In addition, we should take the possible AGN contribution to the sub-mm source counts into account, though there are some observational constraints on their fraction in the sources (e.g. Haarsma, Partridge 1998).

Instruments with a much better angular resolution in sub-mm wavelengths, like forthcoming Large Millimeter and Submillimeter Array (LMSA) and further, the international collaboration of large arrays, Atacama Large Millimeter Array (ALMA) will help to solve the confusion problem, and provide much information concerning the high-redshift status of galaxies. We stress that large-area surveys targeted at bright submillimeter sources are also necessary to fix the evolution at $1 \lesssim z \lesssim 2$ (for the detailed examination of this issue, see Takeuchi et al. 2000c and Hughes 2000).

5. Discussion

5.1. Implication: High or Low Redshift?

Our analysis shows that the steep slope of the IR number counts and the peak intensity of the CIRB can be attributed to relatively low-redshift ($0.5 < z < 1$) galaxies. Previous studies of the redshift distribution of IR galaxies based on the CIRB spectrum and IR number counts tend to claim that the IR–sub-mm observations support a model of high star-formation rate (SFR) at a large redshift ($z > 2$), and consequently imply a large number of heavily obscured distant galaxies. We focus on this issue and examine our results in this subsection.

We first took care of the CIRB intensity at 140 μm (Hauser et al. 1998). As discussed in section 3, the observation and calibration of COBE DIRBE at this wavelength is sufficiently reliable. Therefore, it seems strange that most of the previous studies completely ignored this observed point, but focused on other points. Moreover, some previous model predictions failed to reproduce the overall spectral shape of the CIRB. If we use the normal dust temperature, $T_{\rm dust} = 30$–$40\,{\rm K}$, the spectral shape of the CIRB naturally requires a significant contribution of low-z IR galaxies.

Gispert, Lagache, and Puget (2000) coherently analysed the cosmic background from optical to millimeter wavelengths and derived the cosmic SFH, and also found a rapid increase of cosmic luminosity density, and consequently, the cosmic SFR density. They also found that the contribution of the low-z IR galaxies to the CIRB around the peak is almost 100%. Their evolution of the cosmic luminosity density at $z < 1$ is quite consistent with our result. Eales et al. (1999) studied their sub-mm survey and presented a similar SFH, although their peak of the SFH is located on slightly higher redshift.

Recently, Scott et al. (2000) performed a sub-mm follow-up observation of 10 known FIRBACK 170-μm sources and reported some detections at 450 and 850 μm. They found that the sub-mm fluxes of the FIRBACK sources are fairly weak. We see in their figure 1 that the SEDs of these sources are consistent with those of IR galaxies at $0 < z < 0.5$. Scott et al. (2000) mentioned that there remains a degree of freedom to hypothesize the very hot $T_{\rm dust}$. They carefully considered another redshift estimation, a variation in the dust emissivity and dust temperature, and concluded that these sources have redshifts of $0 < z < 1.5$, which agrees well with our result.

Juvela et al. (2000) reported the result of a galaxy count as a part of their ISOPHOT CIRB project. They performed multi-band surveys at wavelengths of 90 μm, 150 μm, and 180 μm; a relatively high source surface density suggested strong galaxy evolution. They compared the observed SEDs of the newly detected ISO sources with the IR-luminous galaxy SEDs of Lisenfeld, Isaak, and Hills (2000), and found that the SEDs of the detected objects are consistent with those of dusy galaxies at redshifts $0.5 \lesssim z \lesssim 1$. This also supports our estimated evolution of IR galaxies.

We must note that, in addition, the density parameter of the Universe $\Omega_0 = 1$ often assumed in many previous models. A large Ω_0 suppresses the faintest slope of the galaxy number count and the intensity of the CIRB (e.g. Takeuchi et al. 1999). Therefore, a group of models which prefer very high redshift IR galaxies can be reconciled with the limits of the FIRAS CIRB spectrum by the large cosmic density. On the other hand, the cosmological constant λ_0 does not significantly affect the model predictions of the CIRB and IR galaxy number counts, compared with the effect of Ω_0. When we use the low-Ω_0 cosmology ($0.2 < \Omega < 0.3$), which is now regarded as being highly plausible, the CIRB spectrum turns out to be a meaningful observational constraint of galaxies at high redshift.

5.2. Cosmic Star Formation History

In this subsection we discuss the star-formation rate per comoving density as a function of the redshift. This is generally called the cosmic star formation history (SFH). Since, as we mentioned in section 1, the FIR luminosity of a galaxy is related to its star-formation rate (SFR; e.g. Kennicutt 1998), we make attempts to convert the FIR luminosity density derived in the previous sections to the SFR density in the Universe.

First, we estimate the comoving luminosity density in the FIR range of 40–120 μm, $\rho_{\rm FIR}(40\text{–}120)$. Using the well-accepted formula presented in the appendix of Helou et al. (1988), $\rho_{\rm FIR}(40\text{–}120)$ is approximated as

$$\rho_{\rm FIR}(40\text{–}120) = 3.26 \times 10^{-19} \times [2.58\rho_\nu(60) + 1.00\rho_\nu(100)]\ [L_\odot\ {\rm Mpc}^{-3}], \quad (11)$$

where $\rho_\nu(60)$ and $\rho_\nu(100)$ are the comoving luminosity density per unit frequency at 60 μm and 100 μm [erg s^{-1}Hz^{-1}Mpc^{-3}], respectively. Helou et al. (1988) asserted that the relation in their appendix is valid in the range of dust temperature T_d and emissivity index γ expected for a galaxy. Thus, we expect that equation (11) is applicable to the FIR luminosity density of the Universe, since the FIR emission originates from dust in galaxies. We show the history of $\rho_{\rm FIR}(40\text{–}120)$ in figure 9. Here, we note that both $\rho_\nu(60)$ and $\rho_\nu(100)$ at redshift z are calculated from the LF and SEDs shown in section 2.

Next, $\rho_{\rm FIR}(40\text{–}120)$ is converted to the SFR per unit comoving volume, $\rho_{\rm SFR}$. Recently, Inoue, Hirashita, and Kamaya (2000) derived the conversion formula from FIR luminosity to the SFR. Their formula is applied to the relation between $\rho_{\rm FIR}(40\text{–}120)$ and $\rho_{\rm SFR}$ as

$$\rho_{\rm SFR}\ [M_\odot\ {\rm yr}^{-1}\ {\rm Mpc}^{-3}] = \frac{2.4 \times 10^{-10}(1-\eta)}{0.4 - 0.2f + 0.6\epsilon}\,\rho_{\rm FIR}(40\text{–}120)\ [L_\odot\ {\rm Mpc}^{-3}], \quad (12)$$

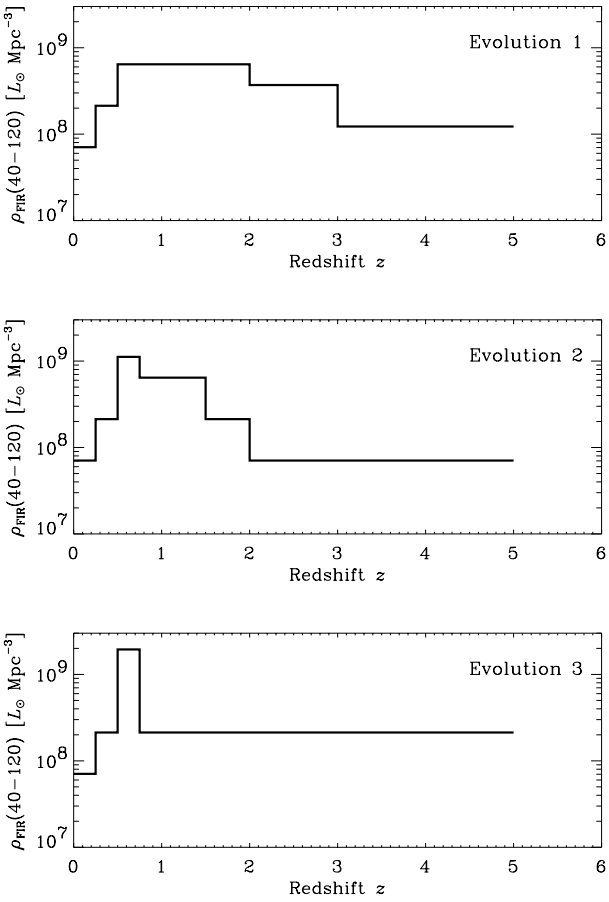

Fig. 9. Evolution of the far-infrared luminosity density within the wavelength range from 40 μm to 120 μm, $\rho_{\rm FIR}(40–120)$. The integrated luminosity density is derived from the monochromatic luminosity density in two IRAS wavebands, $\rho_{60\,\mu{\rm m}}$ and $\rho_{100\,\mu{\rm m}}$ with formula of Helou et al. (1988).

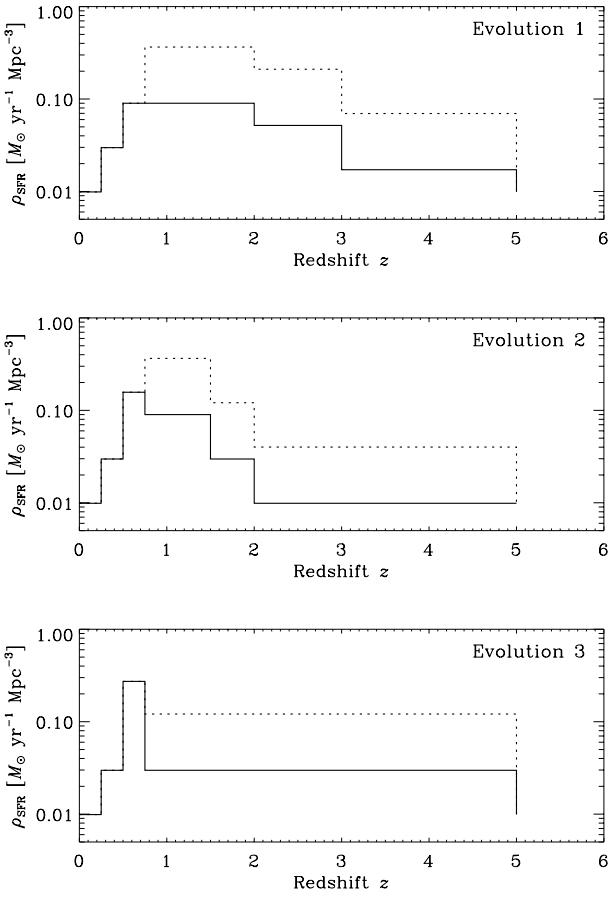

Fig. 10. Star-formation history derived form cosmic infrared background and IR number counts. The solid line represents the case where the factor $C_{\rm FIR}$ for the conversion from FIR luminosity to SFR is fixed at the value corresponding to the solar metallicity. The dotted line presents the case $C_{\rm FIR}$ is 4.1 times larger because of the inefficient conversion from stellar luminosity to FIR luminosity.

where f is the fraction of ionizing photons absorbed by neutral hydrogen [i.e. $(1-f)$ is the fraction of ionizing photons absorbed by dust grains], ϵ is the efficiency of dust absorption for nonionizing photons, and η is the cirrus fraction of observed FIR luminosity. Since Inoue et al.'s expression is based on the luminosity in the range of 8–1000 μm, we have converted it to the luminosity in 40–120 μm by a factor of 1.4 (e.g. Buat, Xu 1996). For convenience of discussion, we define the factor $C_{\rm FIR}$ as

$$C_{\rm FIR}\ [M_\odot\ L_\odot^{-1}\ {\rm yr}^{-1}] = \frac{2.4\times10^{-10}(1-\eta)}{0.4-0.2f+0.6\epsilon}\ , \tag{13}$$

or equivalently

$$\rho_{\rm SFR}\ [M_\odot\ {\rm yr}^{-1}\ {\rm Mpc}^{-3}] = C_{\rm FIR}\cdot\rho_{\rm FIR}(40–120)\ [L_\odot\ {\rm Mpc}^{-3}]\ . \tag{14}$$

The above parameters, f and ϵ, depend on the dust-to-gas ratio, which is related to the metallicity (e.g. Hirashita 1999). Thus, $C_{\rm FIR}$ depends on the metallicity (Hirashita et al. 2000) and varies as the metallicity evolution of galaxies. As the metallicity evolves from 0.01 to 1 times the solar value, $C_{\rm FIR}$ changes from $5.8\times10^{-10}\ M_\odot\ L_\odot^{-1}\ {\rm yr}^{-1}$ to $1.4\times10^{-10}\ M_\odot\ L_\odot^{-1}\ {\rm yr}^{-1}$. This is because the conversion efficiency from the stellar luminosity to the FIR luminosity increases as the dust-to-gas ratio (metallicity) becomes large. For simplicity, the cirrus fraction is set constant as $\eta = 0.5$, since as stated in Hirashita et al. (2000), it is difficult to relate η to the metallicity based on our present knowledge.

In figure 10, we show the derived cosmic SFH. The solid line indicates the history determined by using constant $C_{\rm FIR}$, where the value for the solar metallicity is adopted (i.e., $C_{\rm FIR} = 1.4\times10^{-10}\ [M_\odot\ L_\odot^{-1}\ {\rm yr}^{-1}]$). The dotted line represents the history by using $C_{\rm FIR} = 1.4\times10^{-10}\ [M_\odot\ L_\odot^{-1}\ {\rm yr}^{-1}]$ for $z<1$, while $C_{\rm FIR} = 5.8\times10^{-10}\ [M_\odot\ L_\odot^{-1}\ {\rm yr}^{-1}]$ for $z>1$ to examine the extremely metal-poor case. In order to be consistent, we should model the cosmic chemical evolution. However, since the model produces further undetermined parameters, we do not treat such a model in this paper. We leave detailed and consistent modeling as future works [for reference on the cosmic chemical evolution, see e.g., Pei, Fall, and Hauser (1999)]. We should also decrease η as the FIR luminosity density increases, since the contribution from the cirrus component becomes smaller as the infrared luminosity be-

comes larger (e.g., Beichman, Helou 1991). If η is set to 0 for an extreme case, $C_{\rm FIR}$ becomes two-times larger than that estimated above. Accordingly, the uncertainty of the $C_{\rm FIR}$ induced by the cirrus fraction is estimated to be a factor of two.

In a realistic situation, we expect that the cosmic SFH lies between these two lines in figure 10. In summary, we conclude that $\rho_{\rm SFR}$ increases to $\sim 10^{-1}\ M_\odot\,{\rm yr}^{-1}{\rm Mpc}^{-3}$ at $z \sim 1$ and remains almost constant, or gradually declines for $z > 1$, very similar to the SFH presented in figure 9 of Steidel et al. (1999) and that in figure 6 of Gispert et al. (2000).

6. Summary and Conclusion

We estimated the galaxy evolution from the infrared (IR) galaxy number count and the cosmic infrared background (CIRB). We constructed an empirical galaxy count model based on the spectral energy distributions (SEDs) and luminosity function (LF), both of which are constructed from the IRAS results. The SEDs are made based on the IRAS color–luminosity relations and a tight far-IR–radio correlation. Using this model we estimated the plausible evolution of galaxies from the data in a nonparametric way.

We found that a violent evolution of galaxies as a whole at relatively low redshifts ($z \lesssim 0.5$–0.75) should exist to explain the observed number count of galaxies in the IR wavelengths and the CIRB. Thus, we conclude that the forthcoming galaxy surveys in the IR by future facilities (e.g. ASTRO-F, SOFIA, SIRTF, FIRST, and NGST) have a crucial importance to understand the global history of galaxies, since the IR wavelength is suitable for investigations of the redshift range $0 < z < 1$.

On the other hand, at present, the star formation history at high redshift ($z > 1$) requires further observations and examinations of submillimeter (sub-mm) sources. In addition, source confusion severely affect the flux estimation in sub-mm. Instruments with much better angular resolution at sub-mm wavelengths, like forthcoming LMSA and ALMA, will help to resolve the confusion, and provide much information on the high-redshift status of galaxies. We stress that large-area surveys targeted at bright sub-mm sources are also necessary to fix the evolution at $z \gtrsim 1$–2.

We then converted the FIR luminosity density to the SFR density in the Universe. We estimated the comoving luminosity density in the FIR range of 40–120 μm by the approximate formula of Helou et al. (1988), and $\rho_{\rm FIR}(40$–$120)$ is converted to the star-formation rate per unit comoving volume, $\rho_{\rm SFR}$. We used the conversion formula from FIR luminosity to the SFR derived by Inoue et al. (2000), which took the following three parameters into account: the fraction of ionizing photons absorbed by neutral hydrogen f, the efficiency of dust absorption for nonionizing photons ϵ, and the cirrus fraction of the observed far-infrared luminosity η. Since f and ϵ depend on the dust-to-gas ratio, which is related to the metallicity, we can include the effect of the metal evolution in galaxies. We observe that the SFR density increases to $\sim 10^{-1}\ M_\odot\,{\rm yr}^{-1}{\rm Mpc}^{-3}$ at $z \sim 1$ and that it remains almost constant for $z > 1$, very similar to the star-formation history presented by Steidel et al. (1999) and Gispert et al. (2000).

First we thank an anonymous referee for helpful comments, which improved the quality of the paper. We wish to acknowledge Dr. Hiroshi Shibai, Dr. Mitsunobu Kawada, Dr. Hidenori Takahashi, Dr. Chris P. Pearson, Dr. Hiroshi Matsuo, Dr. Tetsu Kitayama, and Dr. T. N. Rengarajan for helpful discussions and suggestions. HH and KY acknowledge the Research Fellowships of the Japan Society for the Promotion of Science for Young Scientists. We made extensive use of the NASA's Astrophysics Data System Abstract Service (ADS).

Appendix. Performance of the ASTRO-F Far Infrared All-Sky Survey

In this appendix we present the performance of the Japanese ASTRO-F (IRIS) all-sky survey. The bandpass system of the FIR instrument, ASTRO-F Far Infrared Surveyor (FIS) consists of two narrow bands, N60 (50–70 μm) and N170 (150–200 μm), and two wide bands, WIDE-S (50–110 μm) and WIDE-L (110–200 μm). We show the expected number counts at each band in figures 11 and 12. The vertical dot-dot-dot-dashed line presents the 5σ-flux detection limit in each band. The detection limits are estimated as 39 mJy and 110 mJy for N60 and N170, and 16 mJy and 90 mJy for WIDE-S and WIDE-L, respectively (Takahashi et al. 2000). In order to obtain realistic galaxy counts, the wide bandpass wavelength range is involved in the calculation. Figures 11 and 12 show that several $\times 10^5$ galaxies per steradian will be detected by the sets of narrow bandpasses, and roughly 10^6 galaxies per steradian will be detected in WIDE-S and -L.

In order to determine the effect of galaxy evolution from the survey data, a significant sky area should be scanned, to suppress the variation of galaxy surface density. Since galaxies are clustered on the sky, the nominal error bar estimated from the Poisson assumption is an underestimation, and we must take the galaxy angular correlation function into account. Consider a survey area Ω, and divide it into small cells $\{\Delta\Omega_i\}$ so that the number of galaxies in the cell $\{\Delta\Omega_i\}$, $\mathcal{N}_i = 0$ or 1. We set the mean galaxy surface number density $\mathcal{N}$. Then, we have a mean number, $\mathcal{N}_i$, in a solid-angle cell $\Delta\Omega_i$,

$$\langle \mathcal{N}_i \rangle = \mathcal{N}\Delta\Omega_i\ . \tag{A1}$$

By definition, we have $\langle \mathcal{N}_i \rangle = \langle \mathcal{N}_i^2 \rangle = \langle \mathcal{N}_i^3 \rangle = \cdots$. We observe

$$\langle \mathcal{N}_i \mathcal{N}_j \rangle = \mathcal{N}^2[1 + w(\theta_{ij})]\,\Delta\Omega_i\Delta\Omega_j \tag{A2}$$

$$\begin{aligned}
&\langle (\mathcal{N}_i - \langle \mathcal{N}_i \rangle)(\mathcal{N}_j - \langle \mathcal{N}_j \rangle) \rangle \\
&\quad = \langle \mathcal{N}_i \mathcal{N}_j \rangle - \langle \mathcal{N}_i \rangle \langle \mathcal{N}_j \rangle \\
&\quad = \mathcal{N}^2[1 + w(\theta_{ij})]\,\Delta\Omega_i\Delta\Omega_j - \mathcal{N}^2\,\Delta\Omega_i\Delta\Omega_j \\
&\quad = \mathcal{N}^2 w(\theta_{ij})\,\Delta\Omega_i\Delta\Omega_j\ ,
\end{aligned} \tag{A3}$$

where $w(\theta)$ is the angular two-point correlation function of galaxies. Next, we consider the number of galaxies, N, in the survey area Ω. We have

$$\langle N \rangle = \sum_{\Delta\Omega_i \subset \Omega} \langle \mathcal{N}_i \rangle = \int_\Omega \mathcal{N}\, d\Omega = \mathcal{N}\Omega\ , \tag{A4}$$

$$\langle N^2 \rangle = \Big\langle \sum_i \mathcal{N}_i \sum_j \mathcal{N}_j \Big\rangle = \sum_i \langle \mathcal{N}_i^2 \rangle + \sum_{i \neq j} \langle \mathcal{N}_i \mathcal{N}_j \rangle$$

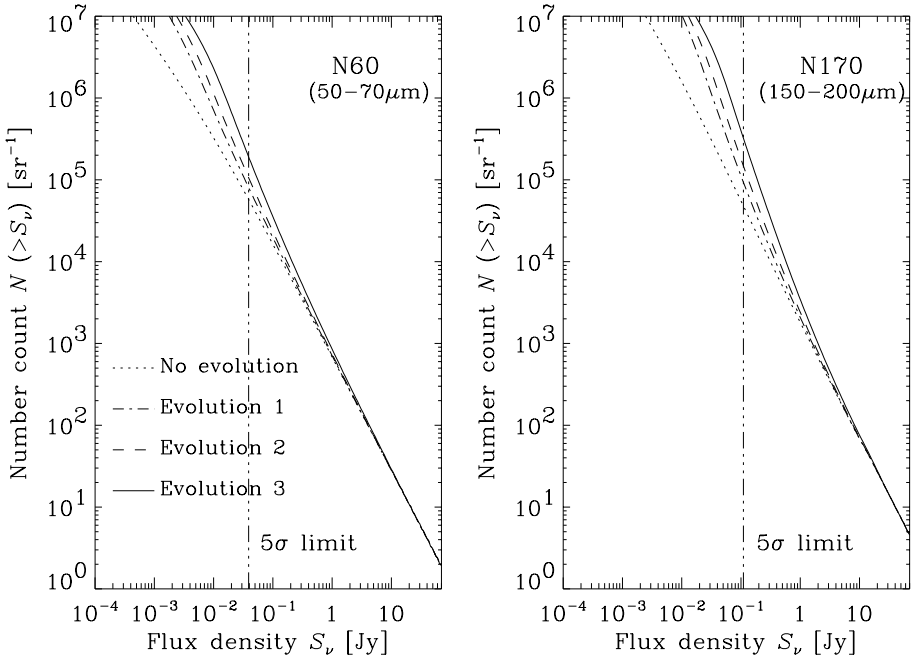

Fig. 11. Expected number counts in the ASTRO-F far-infrared all-sky galaxy survey at two narrow band filters, called N60 and N170. The wavelength ranges are 50–70 μm (N60) and 150–200 μm (N170).

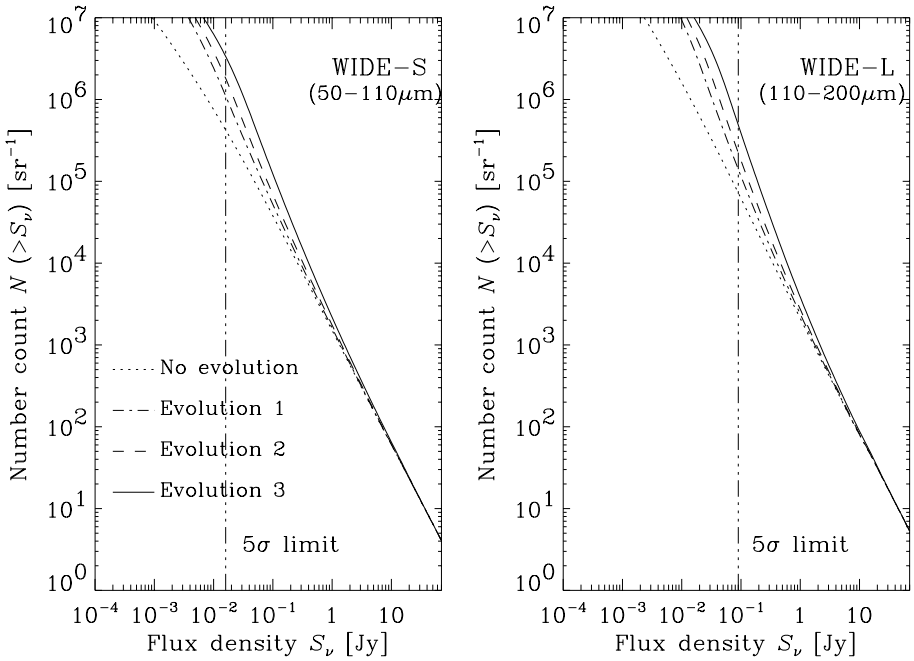

Fig. 12. Expected number counts in the ASTRO-F far-infrared all-sky galaxy survey at two wide band filters, called WIDE-S and WIDE-L. The wavelength ranges are 50–110 μm (WIDE-S) and 110–200 μm (WIDE-L).

$$= \sum_i \langle \mathcal{N}_i \rangle + \sum_{i \neq j} \langle \mathcal{N}_i \mathcal{N}_j \rangle$$
$$= \int_\Omega \mathcal{N} d\Omega + \iint_\Omega \mathcal{N}^2 [1 + w(\theta_{12})]\, d\Omega_1\, d\Omega_2$$
$$= \mathcal{N}\Omega + \mathcal{N}^2\Omega^2 + \mathcal{N}^2 \iint_\Omega w(\theta_{12})\, d\Omega_1\, d\Omega_2\,, \quad \text{(A5)}$$

and thus

$$\langle (N - \langle N \rangle)^2 \rangle = \langle N^2 \rangle - \langle N \rangle^2$$
$$= \mathcal{N}\Omega + \mathcal{N}^2 \iint_\Omega w(\theta_{12})\, d\Omega_1\, d\Omega_2\,. \quad \text{(A6)}$$

If we assume that we take a sufficiently large area than the coherent scale of angular clustering, we can approximate the

above expression as

$$\langle (N - \langle N \rangle)^2 \rangle \simeq \mathcal{N}\Omega + \mathcal{N}^2\Omega \int_\Omega w(\theta)\, d\Omega = \mathcal{N}\Omega \left[1 + \mathcal{N} \int_\Omega w(\theta)\, d\Omega \right]. \quad \text{(A7)}$$

Here, we evaluate the 'signal-to-noise ratio' of the number count S/N,

$$\mathrm{S/N} \equiv \frac{\langle N \rangle}{\sqrt{\langle (N - \langle N \rangle)^2 \rangle}} \simeq \frac{\mathcal{N}\Omega}{\sqrt{\mathcal{N}\Omega \left[1 + \mathcal{N} \int_\Omega w(\theta)\, d\Omega \right]}} \simeq \sqrt{\frac{\Omega}{\int_\Omega w(\theta)\, d\Omega}}. \quad \text{(A8)}$$

We see that the S/N depends on the angular correlation strength and the solid angle of the survey, and is almost independent of the surface density of the sources $\mathcal{N}$. This fact shows that, in order to determine galaxy evolution from number counts, large-area survey is substantially required. The angular correlation function of the IRAS galaxies is $w(\theta) = (\theta/\theta_0)^{-0.66}$ ($\theta_0 = 0.^\circ 11$: Lahav et al. 1990). The angular correlation of galaxies detected by the ASTRO-F survey is obtained by using the scaling relation of $w(\theta)$ with detection limit, through relativistic Limber's equation (e.g. Peebles 1980). If we would like S/N = 10, a survey with $\sim$50–300 deg^2 is required, depending on the considered flux. We can see that, although the deeper is desirable, but *the wider is necessary*. The ASTRO-F all-sky survey promises a unique opportunity to execute such a large-area survey. Thus, we can expect for ASTRO-F survey to distinguish between Evolutions 1, 2, and 3 clearly, and to fix the evolutionary history of IR galaxies up to $z \sim 1$.

References

Allamandola, L. J., Tielens, A. G. G. M., & Barker, J. R. 1989, ApJS, 71, 733

Altieri, B., Metcalfe, L., Kneib, J.-P., McBreen, B., Aussel, H., Biriano, A., Delaney, M., Elbaz, D., et al. 1999, A&A, 343, L65

Ashby, M. L. N., Hacking, P. B., Houck, J. R., Soifer, B. T., & Weisstein, E. W. 1996, ApJ, 456, 428

Aussel, H., Césarsky, C., Elbaz, D., & Starck, J. L. 1999, A&A, 342, 313

Barbosa, D., Bartlett, J. G., Blanchard, A., & Oukbir, J. 1996, A&A, 314, 13

Barger, A. J., Cowie, L. L., & Sanders, D. B. 1999, ApJ, 518, L5

Barger, A. J., Cowie, L. L., Sanders, D. B., Fulton, E., Taniguchi, Y., Sato, Y., Kawara, K., & Okuda, H. 1998, Nature, 394, 248

Beichman, C. A., & Helou, G. 1991, ApJ, 370, L1

Bertin, E., Dennefeld, M., & Moshir, M. 1997, A&A, 323, 685

Blain, A. W., Ivison, R. J., Kneib, J.-P., & Smail, I. 2000, in The Hy-Redshift Universe, ed. A. J. Bunker, & W. J. M. van Breugel, ASP Conf. Ser. 193, 246

Blain, A. W., Kneib, J.-P., Ivison, R. J., & Smail, I. 1999, ApJ, 512, L87

Bregman, J. N., Hogg, D. E., & Roberts, M. S. 1992, ApJ, 387, 484

Buat, V., & Xu, C. 1996, A&A, 306, 61

Clements, D. L., Desert, F. X., Franceschini, A., Reach, W. T., Baker, A. C., Davies, J. K., & Césarsky, C. 1999, A&A, 346, 383

Condon J. J. 1992, ARA&A, 30, 575

Dole, H., Gispert, R., Lagache, G., Puget, J.-L., Aussel, H., Bouchet, F., Ciliegi, P., Clements, D. L., et al. 2000, in ISO Surveys of a Dusty Universe, ed. D. Lemke, M. Stickel, & K. Wilke (Heidelberg: Springer), 54

Dwek, E., Arendt, R. G., Fixsen, D. J., Sodroski, T. J., Odegard, N., Weiland, J. L., Reach, W. T., Hauser, M. G., et al. 1997, ApJ, 475, 565

Eales, S., Lilly, S., Gear, W., Dunne, L., Bond, J. R., Hammer, F., Le Fèvre, O., & Crampton, D. 1999, ApJ, 515, 518

Eales, S., Lilly, S., Webb, T., Dunne, L., Gear, W., Clements, D., & Yun, M. 2000, AJ, 120, 2244

Elbaz, D., Cesarsky, C. J., Fadda, D., Aussel, H., Désert, F. X., Franceschini, A., Flores, H., Harwit, M., et al. 1999, A&A, 351, L37

Fixsen, D. J., Dwek, E., Mather, J. C., Bennett, C. L., & Shafer, R. A. 1998, ApJ, 508, 123

Flores, H., Hammer, F., Désert, F. X., Césarsky, C., Thuan, T., Crampton, D., Eales, S., Le Fèvre, O., et al. 1999a, A&A, 343, 389

Flores, H., Hammer, F., Thuan, T. X., Césarsky, C., Desert, F. X., Omont, A., Lilly, S. J., Eales, S., Crampton, D., & Le Fèvre, O. 1999b, ApJ, 517, 148

Franceschini, A., Mazzei, P., de Zotti, G., & Danese, L. 1994, ApJ, 427, 140

Gardner, J. P. 1998, PASP, 110, 291

Gispert, R., Lagache, G., & Puget, J.-L. 2000, A&A, 360, 1

Guiderdoni, B., Hivon, E., Bouchet, F. R., & Maffei, B. 1998, MNRAS, 295, 877

Haarsma, D. B., & Partridge, R. B. 1998, ApJ, 503, L5

Hauser, M. G., Arendt, R. G., Kelsall, T., Dwek. E., Odegard, N., Weiland, J. L., Freudenreich, H. T., Reach, W. T., et al. 1998, ApJ, 508, 25

Helou, G., Khan, I. R., Malek, L., & Boehmer, L. 1988, ApJS, 68, 151

Helou, G., Soifer, B. T., & Rowan-Robinson, M. 1985, ApJ, 298, L7

Hirashita, H. 1999, ApJ, 510, L99

Hirashita, H., Inoue, A. K., Kamaya, H., & Shibai, H. 2000, A&A, in press, astro-ph/0011237

Hirashita H., Takeuchi, T. T., Ohta, K., & Shibai, H. 1999, PASJ, 51, 81

Hogg, D. W. 2000, AJ, submitted, astro-ph/0004054

Hogg, D. W., & Turner, E. L. 1998, PASP, 110, 727

Holland, W. S., Robson, E. I., Gear, W. K., Cunningham, C. R., Lightfoot, J. F., Jenness, T., Ivison, R. J., Stevens, J. A., et al. 1999, MNRAS, 303, 659

Hughes, D. H. 2000, in Clustering at High Redshift, ed. A. Mazure, O. Le Fèvre, & V. Le Brun, ASP Conf. Ser., 200, 81

Hughes, D. H., & Gaztañaga, E. 2000, in Star Formation from the Small to the Large Scale, ed. F. Favata, A. A. Kaas, & A. Wilson, ESA SP-445, 29

Hughes, D. H., Serjeant, S., Dunlop, J., Rowan-Robinson, M., Blain, A., Mann, R. G., Ivison, R., Peacock, J., et al. 1998, Nature, 394, 241

Inoue, A. K., Hirashita, H., & Kamaya, H. 2000, PASJ, 52,539

Ishii, T. T., Takeuchi, T. T., Hirashita, H., & Yoshikawa, K. 2000, in Star Formation from the Small to the Large Scale, ed. F. Favata, A. A. Kaas, & A. Wilson, ESA SP-445, 421

Juvela, M., Mattila, K., & Lemke, D. 2000, A&A, 360, 813

Kawara, K., Sato, Y., Mastuhara, H., Taniguchi, Y., Okuda, H., Sofue, Y., Matsumoto, T., Wakamatsu, K., et al. 1998, A&A, 336, L9
Kawara, K., Sato, Y., Mastuhara, H., Taniguchi, Y., Okuda, H., Sofue, Y., Matsumoto, T., Wakamatsu, K., et al. 2000, in ISO Surveys of a Dusty Universe, ed. D. Lemke, M. Stickel, & K. Wilke (Heidelberg: Springer), 50
Kennicutt, R. C. Jr. 1998, ARA&A, 36, 189
Kitayama, T., Sasaki, S., & Suto, Y. 1998, PASJ, 50, 1
Lagache, G., Abergel, A., Boulanger, F., Désert, F. X., & Puget, J.-L. 1999, A&A, 344, 322
Lagache, G., Haffner, L. M., Reynolds, R. J., & Tufte, S. L. 2000, A&A, 354, 247
Lahav, O., Nemiroff, R. J., & Piran, T. 1990, ApJ, 350, 119
Lisenfeld, U., Isaak, K. G., & Hills, R. 2000, MNRAS, 312, 433
Malkan, M. A., & Stecker, F. W. 1998, ApJ, 496, 13
Matsuhara, H., Kawara, K., Sato, Y., Taniguchi, Y., Okuda, H., Matsumoto, T., Sofue, Y., Wakamatsu, K., et al. 2000, A&A, 361, 407
Okuda, H. 2000, in ISO Surveys of a Dusty Universe, ed. D. Lemke, M. Stickel, & K. Wilke (Heidelberg: Springer), 40
Oliver, S., Goldshmidt, P., Franceschini, A., Serjeant, S. B. G., Efstathiou, A., Verma, A., Gruppioni, C., Eaton, N., et al. 1997, MNRAS, 289, 471
Oliver, S., Rowan-Robinson, M., Alexander, D. M., Almaini, O., Balcells, M., Baker, A. C., Barcons, X., Barden, M., et al. 2000b, MNRAS, 316, 749
Oliver, S., Serjeant, S., Efstathiou, A., Crockett, H., Gruppioni, C., La Franca, F., et al. 2000a, in ISO Surveys of a Dusty Universe, ed. D. Lemke, M. Stickel, & K. Wilke (Heidelberg: Springer), 28
Pearson, C., Matsuhara, H., Watarai, H., Matsumoto, T., & Onaka, T. 2000, MNRAS, submitted, astro-ph/0008472
Pearson, C., & Rowan-Robinson, M. 1996, MNRAS, 283, 174
Peebles, P. J. E. 1980, The Large-Scale Structure of the Universe (Princeton: Princeton University Press)
Pei, Y. C., Fall, S. M., & Hauser, M. G. 1999, ApJ, 522, 604
Press, W. H., & Schechter, P. 1974, ApJ, 187, 425
Puget, J.-L., Abergel, A., Bernard, J.-P., Boulanger, F., Burton, W. B., Désert, F.-X., & Hartmann, D. 1996, A&A, 308, L5
Puget, J.-L., Abergel, A., Bernard, F., Boulanger, F., Burton, W. B., Desert, F.-X., & Hartmann, D. 1999, A&A, 345, 29
Rowan-Robinson, M., Saunders, W., Lawrence, A., & Leech, K. 1991, MNRAS, 253, 485
Rush, B., Malkan, M. A., & Spinoglio, L. 1993, ApJS, 89, 1
Saunders, W., Rowan-Robinson, M., Lawrence, A., Efstathiou, G., Kaiser, N., Ellis, R. S., & Frenk, C. S. 1990, MNRAS, 242, 318
Scott, D., Lagache, G., Borys, C., Chapman, S. C., Halpern, M., Sajina, A., Ciliegi, P., Clements, D. L., et al. 2000, A&A, 357, L5
Serjeant, S., Oliver, S., Rowan-Robinson, M., Crockett, H., Missoulis, V., Sumner, T., Gruppoini, C., Mann, R. G., et al. 2000, MNRAS, 316, 768
Shibai, H., Okumura, K., & Onaka, T. 2000, in Star Formation 1999, ed. T. Nakamoto (Nobeyama Radio Observatory: NRO), 67
Smail, I., Ivison, R. J., & Blain, A. W. 1997, ApJ, 490, L5
Smith B. J., Kleinman, S. G., Huchra, J. P., & Low, F. J. 1987, ApJ, 318, 161
Soifer B. T., & Neugebauer, G. 1991, AJ, 101, 354
Soifer B. T., Sanders, D. B., Madore, B. F., Neugebauer, G., Danielson, G. E., Elias, J. H., Lonsdale, C. J., & Rice, W. L. 1987, ApJ, 320, 238
Springel, V., & White, S. D. M. 1998, MNRAS, 298, 143
Steidel, C. C., Adelberger, K. L., Giavalisco, M., Dickinson, M., & Pettini, M. 1999, ApJ, 519, 1
Stickel, M., Bogun, S., Lemke, D., Klaas, U., Tóth, L. V., Herbstmeier, U., Richter, G., Assendorp, R., et al. 1998, A&A, 336, 116
Sunyaev, R. A., & Zel'dovich, Ya. B. 1972, Comm. Astrophys. Space Phys. 4, 173
Takahashi, H., Shibai, H., Kawada, M., Hirao, T., Watabe, T., Tsuduku, Y., Nagata, H., Utsuno, H., et al. 2000, in UV, Optical, and IR Space Telescopes and Instruments, ed. J. B. Breckinridge & J. Jacobsen, Proc. SPIE, 4013, 47
Takeuchi T. T., Hirashita, H., Ohta, K., Hattori, T. G., Ishii, T. T., & Shibai, H. 1999, PASP, 111, 288
Takeuchi, T. T., Ishii, T. T., Hirashita, H., Yoshikawa, K., & Mazmine, K. 2000b, in Star Formation 1999, ed. T. Nakamoto (Nobeyama Radio Observatory: NRO), 58
Takeuchi, T. T., Kawabe, R., Kohno, K., Nakanishi, K., Ishii, T. T., Hirashita, H., & Yoshikawa, K. 2000c, PASP, in press
Takeuchi, T. T., Shibai, H., & Ishii, T. T. 2000a, Adv. Space Res., submitted
Tan, J. C., Silk, J., & Balland, C. 1999, ApJ, 522, 579
Xu, C., Hacking, P. B., Fang, F., Shupe, D. L., Lonsdale, C. J., Lu, N. Y., Helou, G., Stacey, G. J., & Ashby, M. L. N. 1998, ApJ, 508, 576